Suplementary material of the article titled: Comparison of Inline and Edge-Illumination X-ray Phase Contrast Imaging for Atherosclerotic Plaque Visualization

1. Multi-material phase retrieval methods with Edge illumination Single Mask and Free-Propagation

Information of the phase shift (ϕ) and the intensity associated with the absorption (I) are related to the real (δ) and imaginary (β) coefficients of the refractive index by means of the following equations

$$\phi\left(\frac{x}{M},\frac{y}{M},0,E\right)=-k(E)\int_{-z_o}^{0}\delta\left(\frac{x}{M},\frac{y}{M},z',E\right)dz' \tag{S1}$$

$$I\left(\frac{x}{M},\frac{y}{M},0,E\right)=I\left(\frac{x}{M},\frac{y}{M},-z_o,E\right)e^{-2k(E)\int_{-z_o}^{0}\beta\left(\frac{x}{M},\frac{y}{M},z',E\right)dz'} \tag{S2}$$

where M is the geometric magnification of the sample at the detector, E is the energy of X-rays through the sample, k is the wavenumber in vacuum and z_o is the thickness of the sample.

X-ray phase contrast methods

Edge illumination Single Mask: EISM

Characteristic equations: Two possible images constructed from an image in EISM, the first obeying equation S3 and the second obeying equation S4.

$$\frac{M^2I_+(x,y,z_1,E)}{I_+\left(\frac{x}{M},\frac{y}{M},-z_o,E\right)}=e^{-2k(E)\int_{-z_o}^{0}\beta\left(\frac{x}{M},\frac{y}{M},z',E\right)dz'}\left[1+\frac{2z_1}{M_1Ak(E)}\frac{\partial\phi\left(\frac{x}{M},\frac{y}{M},0,E\right)}{\partial x'}\right] \tag{S3}$$

$$\frac{M^2I_-(x,y,z_1,E)}{I_-\left(\frac{x}{M},\frac{y}{M},-z_o,E\right)}=e^{-2k(E)\int_{-z_o}^{0}\beta\left(\frac{x}{M},\frac{y}{M},z',E\right)dz'}\left[1-\frac{2z_1}{M_1Ak(E)}\frac{\partial\phi\left(\frac{x}{M},\frac{y}{M},0,E\right)}{\partial x'}\right] \tag{S4}$$

where M_1 is the geometric magnification of each aperture (A) from the EI mask, z_1 is the distance sample-detector, I_+ is the intensity given for one column of pixels and I_- is the intensity given for the neighboring column of pixels.

The traditional method of retrieving the absorption information in EISM is by adding equations S3 and S4 as:

$$e^{-2k(E)\int_{-z_o}^{0}\beta\left(\frac{x}{M},\frac{y}{M},z',E\right)dz'}=\frac{M^2}{2}\left[\frac{I_+(x,y,z_1,E)}{I_+\left(\frac{x}{M},\frac{y}{M},-z_o,E\right)}+\frac{I_-(x,y,z_1,E)}{I_-\left(\frac{x}{M},\frac{y}{M},-z_o,E\right)}\right] \tag{S5}$$

and the differential phase shift by subtracting equations S3 and S4 as:

$$\frac{\partial\phi\left(\frac{x}{M},\frac{y}{M},0,E\right)}{\partial x'}=\frac{M_1Ak(E)}{2z_1}\frac{\left[\frac{I_+(x,y,z_1,E)}{I_+\left(\frac{x}{M},\frac{y}{M},-z_o,E\right)}-\frac{I_-(x,y,z_1,E)}{I_-\left(\frac{x}{M},\frac{y}{M},-z_o,E\right)}\right]}{\left[\frac{I_+(x,y,z_1,E)}{I_+\left(\frac{x}{M},\frac{y}{M},-z_o,E\right)}+\frac{I_-(x,y,z_1,E)}{I_-\left(\frac{x}{M},\frac{y}{M},-z_o,E\right)}\right]} \quad \textbf{(S6)}$$

There are alternative phase retrieval methods in EISM that allow direct mapping of the projected thickness of each material within the sample. These include the Beltrán method.

- **Phase retrieval: Projected thickness maps**

The method starts with equations S1 and S2 within equations S3 and S4, obtaining

$$\frac{M^2I_\pm(x,y,z_1,E)}{I_\pm\left(\frac{x}{M},\frac{y}{M},-z_o,E\right)}=e^{-2k(E)\int_{-z_o}^{0}\beta\left(\frac{x}{M},\frac{y}{M},z',E\right)dz'}\left[1\mp\frac{2z_1}{M_1A}\frac{\partial\int_{-z_o}^{0}\delta\left(\frac{x}{M},\frac{y}{M},z',E\right)dz'}{\partial x'}\right] \quad \textbf{(S7)}$$

The total projected thickness of the sample is defined as

$$a_T\left(\frac{x}{M},\frac{y}{M}\right)=a_1\left(\frac{x}{M},\frac{y}{M}\right)+a_2\left(\frac{x}{M},\frac{y}{M}\right) \quad \textbf{(S8)}$$

where the $a_1\left(\frac{x}{M},\frac{y}{M}\right)$ ($a_2\left(\frac{x}{M},\frac{y}{M}\right)$) refers to the projected thickness of the encasing (encapsulated) material. With equation S8 and the following approximation in the integral terms

$$\int_{-z_o}^{0}\delta\left(\frac{x}{M},\frac{y}{M},z',E\right)dz'=\delta_1(E)a_1\left(\frac{x}{M},\frac{y}{M}\right)+\delta_2(E)a_2\left(\frac{x}{M},\frac{y}{M}\right)$$

$$\int_{-z_o}^{0}\delta\left(\frac{x}{M},\frac{y}{M},z',E\right)dz'=\delta_1(E)a_T\left(\frac{x}{M},\frac{y}{M}\right)+\Delta\delta(E)a_2\left(\frac{x}{M},\frac{y}{M}\right) \quad \textbf{(S9)}$$

$$\int_{-z_o}^{0}\beta\left(\frac{x}{M},\frac{y}{M},z',E\right)dz'=\beta_1(E)a_1\left(\frac{x}{M},\frac{y}{M}\right)+\beta_2(E)a_2\left(\frac{x}{M},\frac{y}{M}\right)$$

$$\int_{-z_o}^{0}\beta\left(\frac{x}{M},\frac{y}{M},z',E\right)dz'=\beta_1(E)a_T\left(\frac{x}{M},\frac{y}{M}\right)+\Delta\beta(E)a_2\left(\frac{x}{M},\frac{y}{M}\right) \quad \textbf{(S10)}$$

where $\Delta\delta(E)=\delta_2(E)-\delta_1(E)$ and $\Delta\beta(E)=\beta_2(E)-\beta_1(E)$, equation S7 is written as

$$\frac{M^2I_\pm(x,y,z_1,E)}{I_\pm\left(\frac{x}{M},\frac{y}{M},-z_o,E\right)}=e^{-2k(E)\beta_1(E)a_T\left(\frac{x}{M},\frac{y}{M}\right)}e^{-2k(E)\Delta\beta(E)a_{2\pm}\left(\frac{x}{M},\frac{y}{M}\right)}\left[1\mp\frac{2z_1}{M_1A}\delta_1(E)\frac{\partial a_T\left(\frac{x}{M},\frac{y}{M}\right)}{\partial x'}\mp\frac{2z_1}{M_1A}\Delta\delta(E)\frac{\partial a_{2\pm}\left(\frac{x}{M},\frac{y}{M}\right)}{\partial x'}\right] \quad \textbf{(S11)}$$

Assuming that the total projected thickness slowly varies along the transversal plane, then $\vec{\nabla}_T a_T\left(\frac{x}{M},\frac{y}{M}\right) \approx 0 \rightarrow \frac{\partial a_T\left(\frac{x}{M'}\frac{y}{M}\right)}{\partial x'} \approx 0$. Although that assumption is violated at the edges of the sample, the retrieving of the projected thickness of the encapsulated material is valid only if it is not located close to the edges. Consequently, equation S11 is

$$\frac{M^2 I_{\pm}(x,y,z_1,E)}{I_{\pm}\left(\frac{x}{M},\frac{y}{M},-z_o,E\right)e^{-2k(E)\beta_1(E)a_T\left(\frac{x}{M'}\frac{y}{M}\right)}} = e^{-2k(E)\Delta\beta(E)a_{2\pm}\left(\frac{x}{M'}\frac{y}{M}\right)}\left[1 \mp \frac{2z_1\Delta\delta(E)}{M_1 A}\frac{\partial a_{2\pm}\left(\frac{x}{M},\frac{y}{M}\right)}{\partial x'}\right] \quad \textbf{(S12)}$$

$$\frac{M^2 I_{\pm}(x,y,z_1,E)}{I_{\pm}\left(\frac{x}{M},\frac{y}{M},-z_o,E\right)e^{-2k(E)\beta_1(E)a_T\left(\frac{x}{M'}\frac{y}{M}\right)}} = \left[1 \pm \frac{z_1\Delta\delta(E)}{M_1 Ak(E)\Delta\beta(E)}\frac{\partial}{\partial x'}\right]e^{-2k(E)\Delta\beta(E)a_{2\pm}\left(\frac{x}{M'}\frac{y}{M}\right)} \quad \textbf{(S13)}$$

where $\frac{\partial}{\partial x'}e^{-2k(E)\Delta\beta(E)a_{2\pm}\left(\frac{x}{M'}\frac{y}{M}\right)} = -2k(E)\Delta\beta(E)\frac{\partial a_{2\pm}\left(\frac{x}{M'}\frac{y}{M}\right)}{\partial x'}e^{-2k(E)\Delta\beta(E)a_{2\pm}\left(\frac{x}{M'}\frac{y}{M}\right)}$. Using Fourier space enables to convert the differential equations S13 into algebraic equations. Supposing a discrete system $N \times \frac{N}{2}$ pixels in the detector, with each pixel as a square of size W, the discrete Fourier transforms of each function from equation S13 are

$$F_{\pm}(x,y,E) = \frac{M^2 I_{\pm}(x,y,z_1,E)}{I_{\pm}\left(\frac{x}{M},\frac{y}{M},-z_o,E\right)e^{-2k(E)\beta_1(E)a_T\left(\frac{x}{M'}\frac{y}{M}\right)}} = \frac{2}{N^2}\sum_{u=-\frac{N}{4}}^{\frac{N}{4}}\sum_{v=-\frac{N}{2}}^{\frac{N}{2}} f_{\pm}(u,v,E)e^{\frac{2\pi i}{N}(xu+yv)} \quad \textbf{(S14)}$$

$$G_{\pm}(x,y,E) = e^{-2k(E)\Delta\beta(E)a_{2\pm}\left(\frac{x}{M'}\frac{y}{M}\right)} = \frac{2}{N^2}\sum_{u=-\frac{N}{4}}^{\frac{N}{4}}\sum_{v=-\frac{N}{2}}^{\frac{N}{2}} g_{\pm}(u,v,E)e^{\frac{2\pi i}{N}(xu+yv)} \quad \textbf{(S15)}$$

with u and v as the Fourier frequencies associated to x and y, respectively. A second-order Taylor expansion is used around the center of mass of an arbitrary pixel (x,y) to calculate the function $G_{\pm}$ in the center of mass of its neighbor pixels, at $(x \pm 2W, y)$, and the derivative of $G_{\pm}$ as

$$G_{\pm}(x \pm 2W,y,E) = G_{\pm}(x,y,E) \pm 2W\frac{\partial G_{\pm}(x,y,E)}{\partial x'} + \frac{4W^2}{2}\frac{\partial^2 G_{\pm}(x,y,E)}{\partial x'^2} \quad \textbf{(S16)}$$

$$\frac{\partial G_{\pm}(x,y,E)}{\partial x'} = \frac{1}{4W}[G_{\pm}(x+2W,y,E) - G_{\pm}(x-2W,y,E)] \quad \textbf{(S17)}$$

$$\frac{\partial G_{\pm}(x,y,E)}{\partial x'} = \frac{2}{4WN^2}\left[\sum_{u=-\frac{N}{4}}^{\frac{N}{4}}\sum_{v=-\frac{N}{2}}^{\frac{N}{2}} g_{\pm}(u,v,E)e^{\frac{2\pi i}{N}([x+2W]u+yv)} - \sum_{u=-\frac{N}{4}}^{\frac{N}{4}}\sum_{v=-\frac{N}{2}}^{\frac{N}{2}} g_{\pm}(u,v,E)e^{\frac{2\pi i}{N}([x-2W]u+yv)}\right] \quad \textbf{(S18)}$$

$$\frac{\partial G_{\pm}(x,y,E)}{\partial x'} = \frac{2}{4WN^2}\sum_{u=-\frac{N}{4}}^{\frac{N}{4}}\sum_{v=-\frac{N}{2}}^{\frac{N}{2}}\left[e^{\frac{4\pi i}{N}Wu} - e^{-\frac{4\pi i}{N}Wu}\right]g_{\pm}(u,v,E)e^{\frac{2\pi i}{N}(xu+yv)} \quad \textbf{(S19)}$$

$$\frac{\partial G_{\pm}(x,y,E)}{\partial x'} = \frac{2}{N^2}\sum_{u=-\frac{N}{4}}^{\frac{N}{4}}\sum_{v=-\frac{N}{2}}^{\frac{N}{2}}\frac{i}{2W}\sin\left(\frac{4\pi Wu}{N}\right)g_{\pm}(u,v,E)e^{\frac{2\pi i}{N}(xu+yv)} \quad \textbf{(S20)}$$

With equations S14, S15 and S20, equation S13 is expressed as

$$\frac{2}{N^2}\sum_{u=-\frac{N}{4}}^{\frac{N}{4}}\sum_{v=-\frac{N}{2}}^{\frac{N}{2}} f_{\pm}(u,v,E)e^{\frac{2\pi i}{N}(xu+yv)} = \frac{2}{N^2}\sum_{u=-\frac{N}{4}}^{\frac{N}{4}}\sum_{v=-\frac{N}{2}}^{\frac{N}{2}}\left[1 \pm \frac{iz_1\Delta\delta(E)}{2WM_1Ak(E)\Delta\beta(E)}\sin\left(\frac{4\pi Wu}{N}\right)\right] g_{\pm}(u,v,E)e^{\frac{2\pi i}{N}(xu+yv)}$$

$$f_{\pm}(u,v,E) = \left[1 \pm \frac{iz_1\Delta\delta(E)}{2WM_1Ak(E)\Delta\beta(E)}\sin\left(\frac{4\pi Wu}{N}\right)\right] g_{\pm}(u,v,E)$$

$$g_{\pm}(u,v,E) = \frac{f_{\pm}(u,v,E)}{1 \pm \frac{iz_1\Delta\delta(E)}{2WM_1Ak(E)\Delta\beta(E)}\sin\left(\frac{4\pi Wu}{N}\right)} \quad \textbf{(S21)}$$

allowing to calculate $a_{2\pm}\left(\frac{x}{M},\frac{y}{M}\right)$ from $g_{\pm}(u,v,E)$ in equations S15 as

$$e^{-2k(E)\Delta\beta(E)a_{2\pm}\left(\frac{x}{M},\frac{y}{M}\right)} = \frac{2}{N^2}\sum_{u=-\frac{N}{4}}^{\frac{N}{4}}\sum_{v=-\frac{N}{2}}^{\frac{N}{2}}\left[\frac{f_{\pm}(u,v,E)}{1 \pm \frac{iz_1\Delta\delta(E)}{2WM_1Ak(E)\Delta\beta(E)}\sin\left(\frac{4\pi Wu}{N}\right)}\right] e^{\frac{2\pi i}{N}(xu+yv)}$$

$$a_{2\pm}\left(\frac{x}{M},\frac{y}{M}\right) = -\frac{1}{2k(E)\Delta\beta(E)}\ln\left[\frac{2}{N^2}\sum_{u=-\frac{N}{4}}^{\frac{N}{4}}\sum_{v=-\frac{N}{2}}^{\frac{N}{2}}\left[\frac{f_{\pm}(u,v,E)}{1 \pm \frac{iz_1\Delta\delta(E)}{2WM_1Ak(E)\Delta\beta(E)}\sin\left(\frac{4\pi Wu}{N}\right)}\right] e^{\frac{2\pi i}{N}(xu+yv)}\right]$$

(S22)

From equations S22, two estimates of the projected thickness of the encapsulated material can be obtained. Its total projected thickness can be estimated by averaging the two projected thicknesses as:

$$a_2\left(\frac{x}{M},\frac{y}{M}\right) = \frac{1}{2}\left[a_{2+}\left(\frac{x}{M},\frac{y}{M}\right) + a_{2-}\left(\frac{x}{M},\frac{y}{M}\right)\right] \quad \textbf{(S23)}$$

Verification

Monochromatic images were acquired for a PMMA tube (diameter of 3.85 mm) with two inner tubes (diameters of 0.92 mm), made of Alumina and hydroxyapatite (HA). The corresponding imaging energies were 20 keV, 25 keV and 30 keV (Figure 1), a sample-detector of 0.6 m (z_1), an X-ray source-sample distance of 0.6, and 5 dithering steps. The objective is to retrieve the projected thickness of Alumina ($\Delta\delta(E) = \delta_{Al}(E) - \delta_{PMMA}(E)$ and $\Delta\beta(E) = \beta_{Al}(E) - \beta_{PMMA}(E)$) and HA ($\Delta\delta(E) = \delta_{HA}(E) - \delta_{PMMA}(E)$ and $\Delta\beta(E) = \beta_{HA}(E) - \beta_{PMMA}(E)$), using equations S22 and S23. The pixel size was $W = 55\ \mu$m.

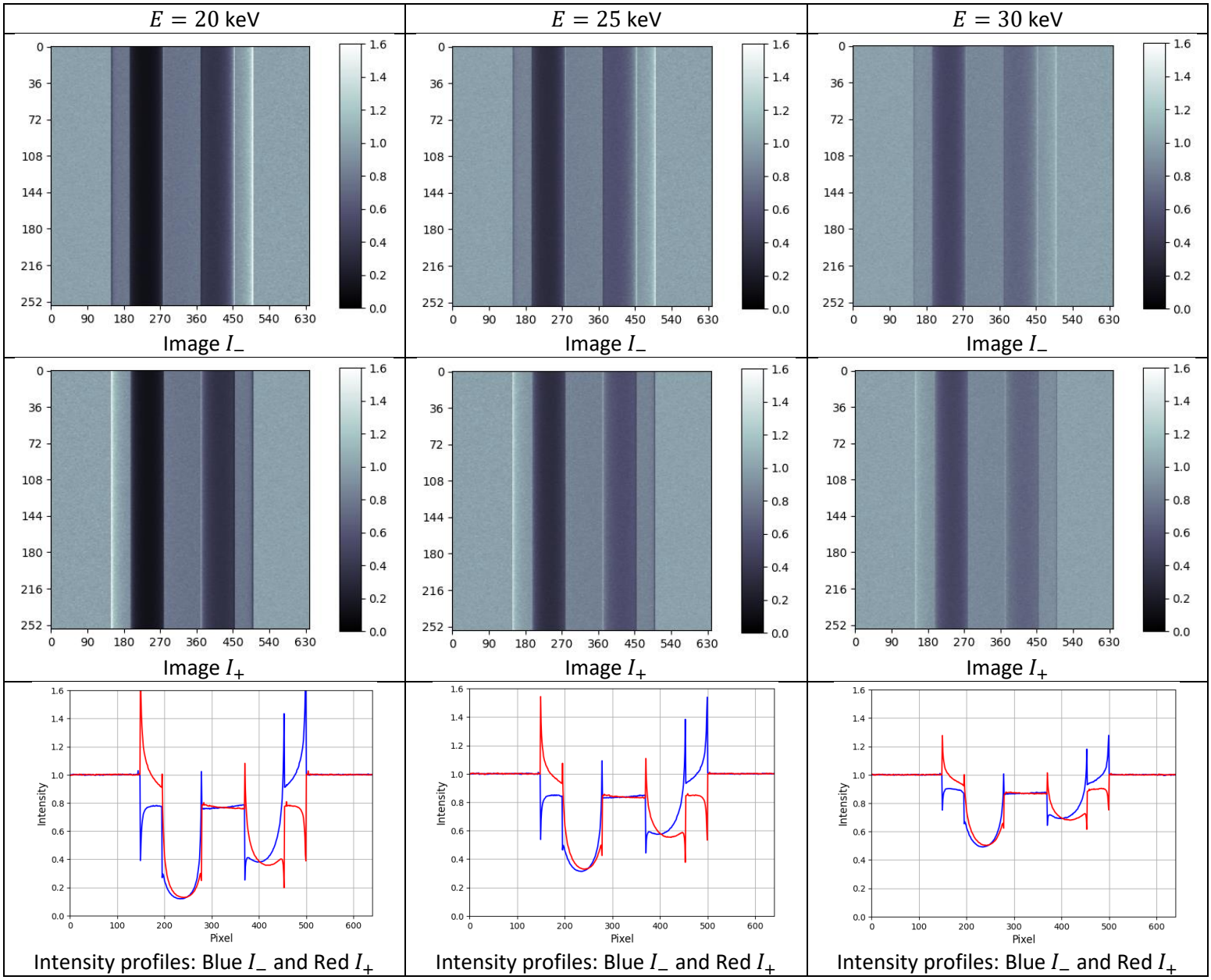

Figure S1. Images at 20, 25 and 30 keV using EISM. Intensity profiles from the image I_- (blue solid lines) and the image I_+ (red solid lines) are presented in the third row.

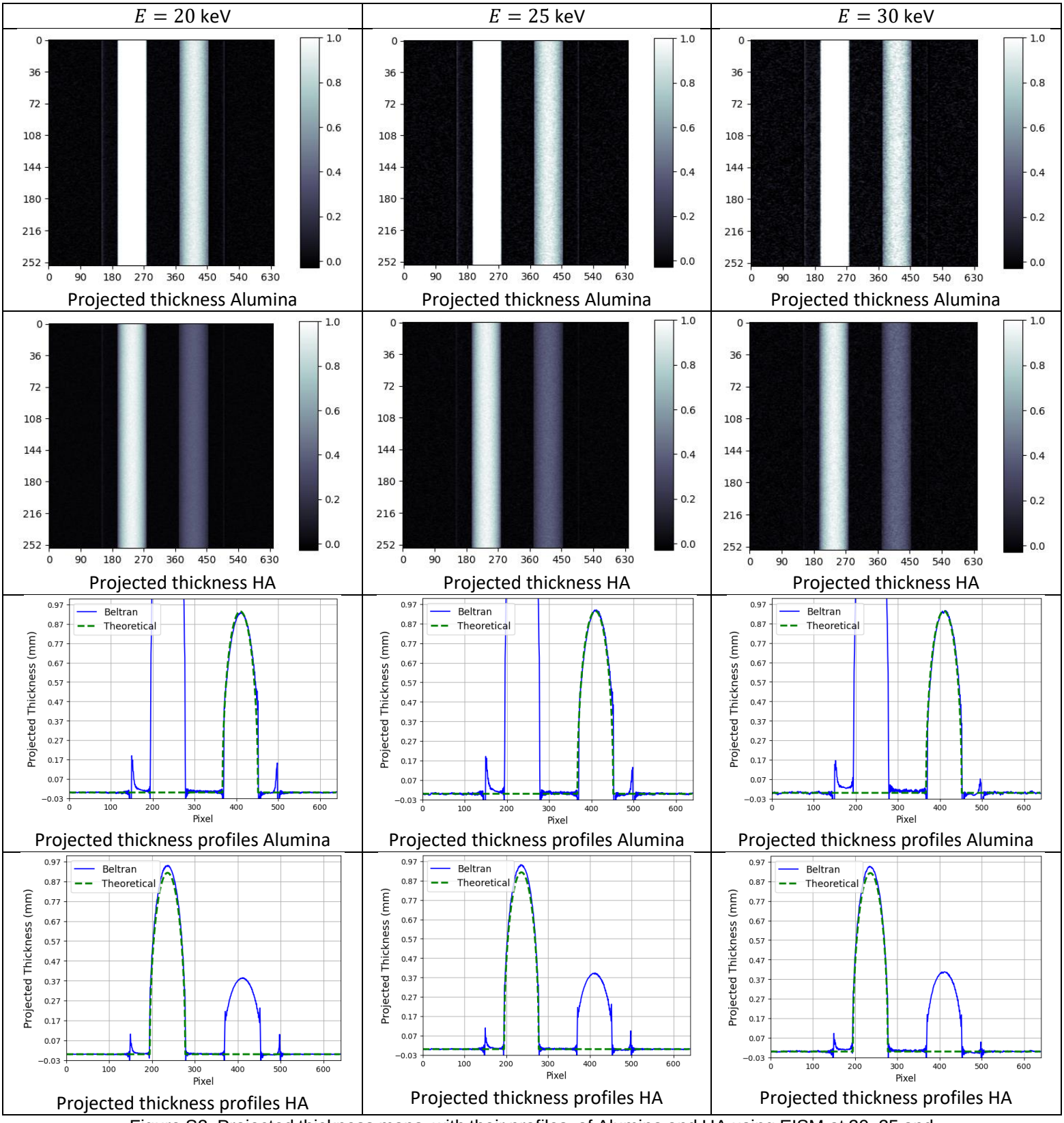

Figure S2. Projected thickness maps, with their profiles, of Alumina and HA using EISM at 20, 25 and 30 keV. Recovered projected thickness profiles (blue solid lines) are compared with the expected profiles (green dotted lines).

Free Propagation (Inline XPCI)

Characteristic equation: Transport-Intensity equation

$$M^2 I(x,y,z_1,E) = I\left(\frac{x}{M},\frac{y}{M},0,E\right) - \frac{z_1}{Mk(E)}\vec{\nabla}_T \cdot \left[I\left(\frac{x}{M},\frac{y}{M},0,E\right)\vec{\nabla}_T \phi\left(\frac{x}{M},\frac{y}{M},0,E\right)\right] \quad \textbf{(S24)}$$

$$\frac{M^2 I(x,y,z_1,E)}{I\left(\frac{x}{M},\frac{y}{M},-z_o,E\right)} = \left[e^{-2k(E)\int_{-z_o}^{0}\beta\left(\frac{x}{M},\frac{y}{M},z',E\right)dz'} + \frac{z_1}{M}\vec{\nabla}_T \cdot \left[e^{-2k(E)\int_{-z_o}^{0}\beta\left(\frac{x}{M},\frac{y}{M},z',E\right)dz'}\vec{\nabla}_T \int_{-z_o}^{0}\delta\left(\frac{x}{M},\frac{y}{M},z',E\right)dz'\right]\right] \quad \textbf{(S25)}$$

using equations S1 and S2 in equation S25.

- **Phase retrieval: Projected thickness maps**

To retrieve the projected thickness of the encapsulated material using Inline XPCI, equations S9 and S10 in equation S25 are used, again assuming $\vec{\nabla}_T a_T\left(\frac{x}{M},\frac{y}{M}\right) \approx 0$, obtaining

$$\frac{M^2 I(x,y,z_1,E)}{I\left(\frac{x}{M},\frac{y}{M},-z_o,E\right)e^{-2k(E)\beta_1(E)a_T\left(\frac{x}{M},\frac{y}{M}\right)}} = e^{-2k(E)\Delta\beta(E)a_2\left(\frac{x}{M},\frac{y}{M}\right)} + \frac{z_1\Delta\delta(E)}{M}\vec{\nabla}_T \cdot \left[e^{-2k(E)\Delta\beta(E)a_2\left(\frac{x}{M},\frac{y}{M}\right)}\vec{\nabla}_T a_2\left(\frac{x}{M},\frac{y}{M}\right)\right]$$

$$\frac{M^2 I(x,y,z_1,E)}{I\left(\frac{x}{M},\frac{y}{M},-z_o,E\right)e^{-2k(E)\beta_1(E)a_T\left(\frac{x}{M},\frac{y}{M}\right)}} = \left[1 - \frac{z_1\Delta\delta(E)}{2k(E)M\Delta\beta(E)}\nabla_T^2\right]e^{-2k(E)\Delta\beta(E)a_2\left(\frac{x}{M},\frac{y}{M}\right)} \quad \textbf{(S26)}$$

where $\vec{\nabla}_T e^{-2k(E)\Delta\beta(E)a_2\left(\frac{x}{M},\frac{y}{M}\right)} = -2k(E)\Delta\beta(E)e^{-2k(E)\Delta\beta(E)a_2\left(\frac{x}{M},\frac{y}{M}\right)}\vec{\nabla}_T a_2\left(\frac{x}{M},\frac{y}{M}\right)$. Using discrete Fourier space enables to convert the differential equation S26 into an algebraic equation. The discrete Fourier transforms of each function from equation S26 are

$$F(x,y,E) = \frac{M^2 I(x,y,z_1,E)}{I\left(\frac{x}{M},\frac{y}{M},-z_o,E\right)e^{-2k(E)\beta_1(E)a_T\left(\frac{x}{M},\frac{y}{M}\right)}} = \frac{1}{N^2}\sum_{u,v=-\frac{N}{2}}^{\frac{N}{2}} f(u,v,E)e^{\frac{2\pi i}{N}(xu+yv)} \quad \textbf{(S27)}$$

$$G(x,y,E) = e^{-2k(E)\Delta\beta(E)a_2\left(\frac{x}{M},\frac{y}{M}\right)} = \frac{1}{N^2}\sum_{u,v=-\frac{N}{2}}^{\frac{N}{2}} g(u,v,E)e^{\frac{2\pi i}{N}(xu+yv)} \quad \textbf{(S28)}$$

For the Laplacian of the function G, it is considered

$$\nabla_T^2 G(x,y,E) = \frac{\partial^2 G(x,y,E)}{\partial x'^2} + \frac{\partial^2 G(x,y,E)}{\partial y'^2} \quad \textbf{(S29)}$$

A second-order Taylor expansion around the center of mass of an arbitrary pixel (x,y) is used to calculate the function G at the center of mass of its nearest neighboring pixels, at $(x \pm W, y)$ and $(x, y \pm W)$, and to calculate the discrete second derivatives of G as

$$G(x \pm W,y,E) = G(x,y,E) \pm W\frac{\partial G(x,y,E)}{\partial x'} + \frac{W^2}{2}\frac{\partial^2 G(x,y,E)}{\partial x'^2} \quad \textbf{(S30)}$$

$$\frac{\partial^2 G(x,y,E)}{\partial x'^2} = \frac{1}{W^2}[G(x+W,y,E) + G(x-W,y,E) - 2G(x,y,E)] \quad \textbf{(S31)}$$

$$G(x, y \pm W, E) = G(x, y, E) \pm W\frac{\partial G(x, y, E)}{\partial y'} + \frac{W^2}{2}\frac{\partial^2 G(x, y, E)}{\partial y'^2} \quad \textbf{(S32)}$$

$$\frac{\partial^2 G(x, y, E)}{\partial y'^2} = \frac{1}{W^2}[G(x, y + W, E) + G(x, y - W, E) - 2G(x, y, E)] \quad \textbf{(S33)}$$

$$\nabla_T^2 G(x, y, E) = \frac{1}{W^2}[G(x + W, y, E) + G(x - W, y, E) + G(x, y + W, E) + G(x, y - W, E) - 4G(x, y, E)] \quad \textbf{(S34)}$$

$$\nabla_T^2 G(x, y, E) = \frac{1}{W^2 N^2}\left[\sum_{u,v=-\frac{N}{2}}^{\frac{N}{2}}\left[e^{\frac{2\pi i}{N}Wu} + e^{-\frac{2\pi i}{N}Wu}\right] g(u, v, E)e^{\frac{2\pi i}{N}(xu+yv)} + \sum_{u,v=-\frac{N}{2}}^{\frac{N}{2}}\left[e^{\frac{2\pi i}{N}Wv} + e^{-\frac{2\pi i}{N}Wv}\right] g(u, v, E)e^{\frac{2\pi i}{N}(xu+yv)} - \sum_{u,v=-\frac{N}{2}}^{\frac{N}{2}} 4g(u, v, E)e^{\frac{2\pi i}{N}(xu+yv)}\right] \quad \textbf{(S36)}$$

$$\nabla_T^2 G(x, y, E) = \frac{1}{N^2}\sum_{u,v=-\frac{N}{2}}^{\frac{N}{2}} \frac{2}{W^2}\left[\cos\left(\frac{2\pi Wu}{N}\right) + \cos\left(\frac{2\pi Wv}{N}\right) - 2\right] g(u, v, E)e^{\frac{2\pi i}{N}(xu+yv)} \quad \textbf{(S37)}$$

With equations S27, S28 and S37, equation S26 is expressed as

$$\frac{1}{N^2}\sum_{u,v=-\frac{N}{2}}^{\frac{N}{2}} f(u, v, E)e^{\frac{2\pi i}{N}(xu+yv)} = \frac{1}{N^2}\sum_{u,v=-\frac{N}{2}}^{\frac{N}{2}}\left[1 - \frac{z_1\Delta\delta(E)}{W^2 Mk(E)\Delta\beta(E)}\left[\cos\left(\frac{2\pi Wu}{N}\right) + \cos\left(\frac{2\pi Wv}{N}\right) - 2\right]\right] g(u, v, E)e^{\frac{2\pi i}{N}(xu+yv)}$$

$$f(u, v, E) = \left[1 - \frac{z_1\Delta\delta(E)}{W^2 Mk(E)\Delta\beta(E)}\left[\cos\left(\frac{2\pi Wu}{N}\right) + \cos\left(\frac{2\pi Wv}{N}\right) - 2\right]\right] g(u, v, E) \quad \textbf{(S38)}$$

$$g(u, v, E) = \frac{f(u, v, E)}{1 - \frac{z_1\Delta\delta(E)}{W^2 Mk(E)\Delta\beta(E)}\left[\cos\left(\frac{2\pi Wu}{N}\right) + \cos\left(\frac{2\pi Wv}{N}\right) - 2\right]} \quad \textbf{(S39)}$$

allowing to estimate $a_2\left(\frac{x}{M}, \frac{y}{M}\right)$ from $g(u, v, E)$ in equation S28 as

$$e^{-2k(E)\Delta\beta(E)a_2\left(\frac{x}{M}, \frac{y}{M}\right)} = \frac{1}{N^2}\sum_{u,v=-\frac{N}{2}}^{\frac{N}{2}}\left[\frac{f(u, v, E)}{1 - \frac{z_1\Delta\delta(E)}{W^2 Mk(E)\Delta\beta(E)}\left[\cos\left(\frac{2\pi Wu}{N}\right) + \cos\left(\frac{2\pi Wv}{N}\right) - 2\right]}\right] e^{\frac{2\pi i}{N}(xu+yv)}$$

$$a_2\left(\frac{x}{M}, \frac{y}{M}\right) = -\frac{1}{2k(E)\Delta\beta(E)}\ln\left[\frac{1}{N^2}\sum_{u,v=-\frac{N}{2}}^{\frac{N}{2}}\left[\frac{f(u, v, E)}{1 - \frac{z_1\Delta\delta(E)}{W^2 Mk(E)\Delta\beta(E)}\left[\cos\left(\frac{2\pi Wu}{N}\right) + \cos\left(\frac{2\pi Wv}{N}\right) - 2\right]}\right] e^{\frac{2\pi i}{N}(xu+yv)}\right] \quad \textbf{(S40)}$$

Verification

Monochromatic images were acquired for a PMMA tube (diameter of 3.85 mm) with two inner tubes (diameters of 0.92 mm), made of Alumina and hydroxyapatite (HA). The

corresponding imaging energies were 20 keV, 25 keV and 30 keV (Figure 3), a sample-detector of 0.6 m (z_1), and an X-ray source-sample distance of 0.6. The objective is to retrieve the projected thickness of Alumina ($\Delta\delta(E) = \delta_{Al}(E) - \delta_{PMMA}(E)$ and $\Delta\beta(E) = \beta_{Al}(E) - \beta_{PMMA}(E)$) and HA ($\Delta\delta(E) = \delta_{HA}(E) - \delta_{PMMA}(E)$ and $\Delta\beta(E) = \beta_{HA}(E) - \beta_{PMMA}(E)$), using equation S40. The pixel size was $W = 55\ \mu$m.

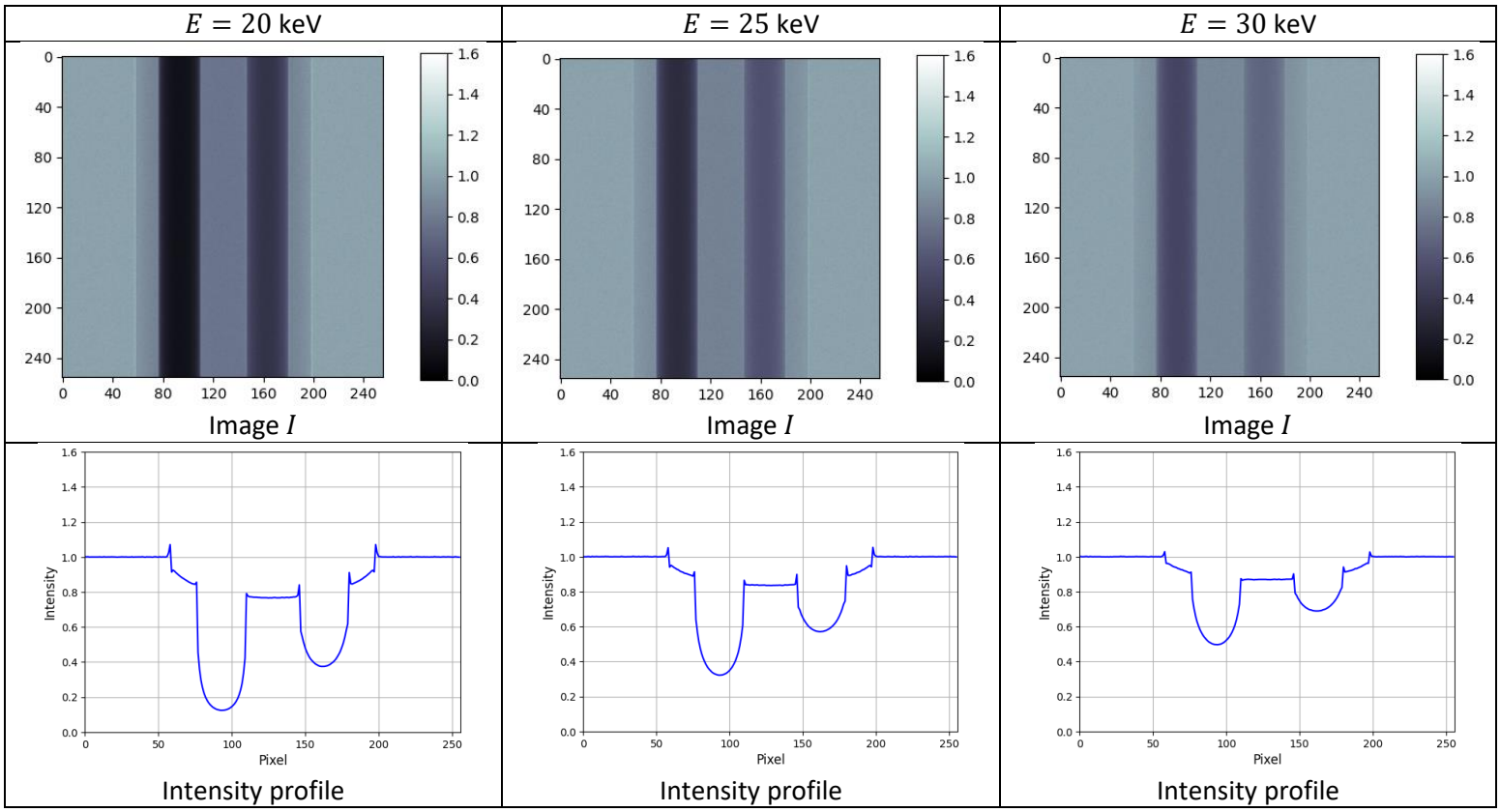

Figure S3. Images at 20, 25 and 30 keV using Inline XPCI. Intensity profiles from the image I (blue solid lines) are presented in the third row.

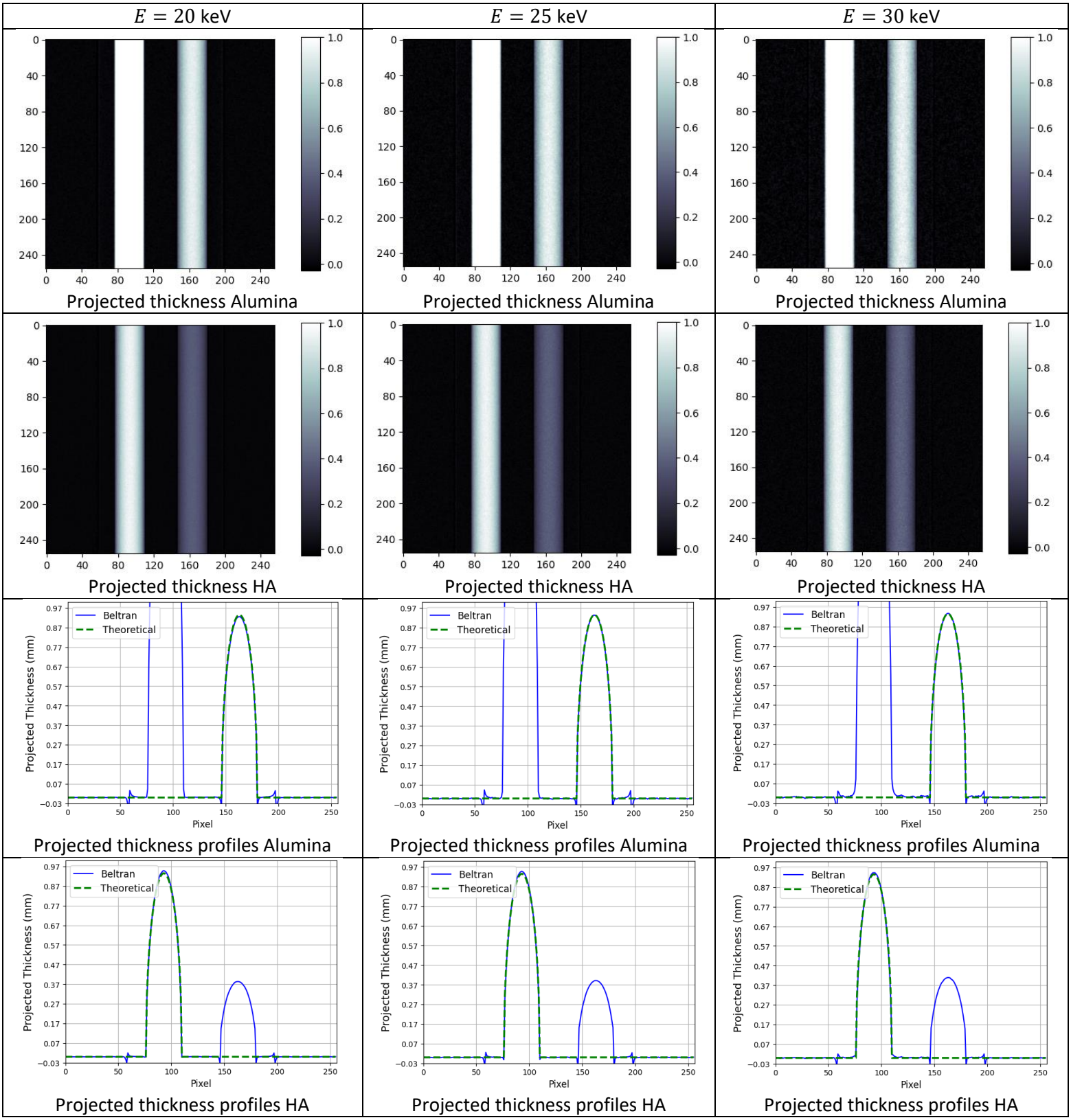

Figure S4. Projected thickness maps, with their profiles, of Alumina and HA using Inline XPCI at 20, 25 and 30 keV. Recovered projected thickness profiles (blue solid lines) are compared with the expected profiles (green dotted lines).

2. Energy resolution of the Timepix3 photon-counting detector

The energy resolution of the detector is determined by the fluorescence spectra of four materials: Zr ($E_{\alpha_1} = 15.775$ keV), Sn ($E_{\alpha_1} = 25.271$ keV), Gd ($E_{\alpha_1} = 42.996$ keV), Am_{241} ($E_{\gamma} = 59.541$ keV), as follows:

- Perform a Gaussian fit around the peaks of the spectrum (Left of Figure S5)
- Obtain σ and E_o from each fit to obtain the energy resolution from each material.
  $\rightarrow R_E = \frac{FWHM}{E_o} = \frac{2\sqrt{2\ln 2}\sigma}{E_o}$
- Graph of R_E vs E (Right of Figure S5)

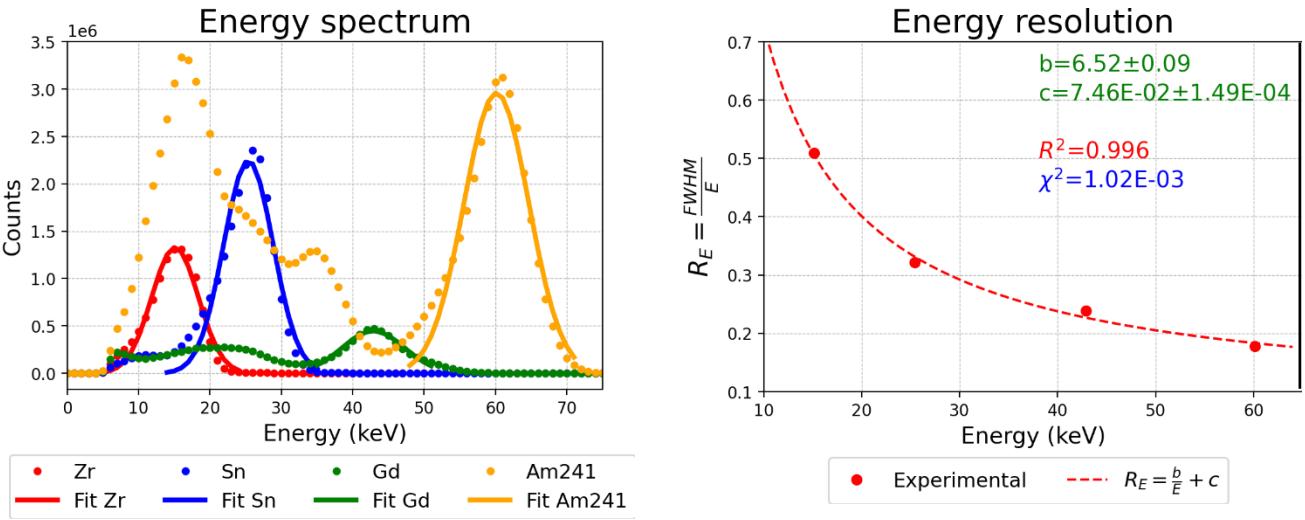

Figure S5. Left. Energy spectrum of four materials, with Gaussian fits. Right. Dependence of Energy resolution of the detector with energy

3. Computational study with larger focal spots and different pixel sizes

The Geant4 framework is again employed to compare Inline XPCI and EISM under conditions with larger focal spot sizes and different pixel sizes. Simulations are performed at two tube voltages (28 kVp and 68 kVp), using a filter of Aluminum 2 mm thick and focal spots of 30 μm and 50 μm. The detector consists of a 256×256 pixel array, with a pixel thickness of 1 mm and pixel pitch of $W = 40$ μm and $W = 123$ μm. The first pitch value is based on the specifications of a CMOS-based flat-panel detector (Hamamatsu C9732DK-11, slightly higher by 10 μm), while the second pitch value corresponds to the flat-panel PaxScan 1313. The same detector material and energy resolution as in the main study are used in these simulations.

The sample is designed as three concentric cylinders: half of the inner cylinder composed of air, and the other half of a PMMA- HA mixture with the following weight ratio: 80% PMMA-20% HA. The intermediate cylinder is composed of PMMA, and the outer cylinder is composed of water. The inner and intermediate cylinders have diameters of z_2 = 0.92 mm and z_3 = 1.94 mm, while the outer cylinder has a diameter of z_o = 6.0 cm. The geometrical parameters to be taken into account throughout the simulation involve defining z_S and z_1, which is z_S = 0.63 m for each method. Three different z_1 values are analyzed: 0.162 m for

the low magnification state (M_{low} = 1.32); 0.57 m for the medium magnification state (M_{medium} = 2.00); and 1.17 m for the high magnification state (M_{high} = 3.00).

To achieve the desired magnification states with both detector pitches in EISM, the following equation:

$$M_{M_1} = \frac{2W}{P} = \frac{z_S + z_1}{z_S - \left[\frac{p}{2} + z_o\right]} \rightarrow P = \frac{2W\left[z_S - \left(\frac{p}{2} + z_o\right)\right]}{z_S + z_1} \quad \textbf{(S41)}$$

is used to calculate the period of the EI mask. Table S1 summarizes the corresponding mask periods for each magnification state, based on the detector pixel pitch used. The spacing between the micrometer gold rods, of thickness p =100 μm, in the EI mask is A_{M_1} =10 μm for each magnification and pixel pitch used.

$W(\mu\text{m})$	z_1(m)	$P(\mu\text{m})$	ξ
40	0.162	57.57	6
40	0.57	37.99	4
40	1.17	25.33	3
123	0.57	116.84	12
123	1.17	77.89	8

Table S1. Mask period and dithering steps according to the magnification state and the detector pixel pitch.

The dithering steps within EISM are also calculated as $\xi = \frac{P}{A_{M_1}}$, with the corresponding periods summarized in Table S1. The case of M_{low} for W =123 μm is excluded due to the excessive computational load associated with the 18 required dithering steps.

The two metrics (contrast and CNR) used in the main document to evaluate visibility in the projected thickness image are also calculated.

The application of equations S22, S23, and S40 allow to generate projected thickness images of the lumen for each voltage, focal spot value, magnification, and pixel pitch. Figure S6 illustrate these results for the focal spot of 30 μm and M_{high} at 28 and 68 kVp, with the first and second rows corresponding to W = 123 μm and W = 40 μm, respectively. In each image, the top half corresponds to the results obtained using equation S40 (Inline XPCI), while the bottom half corresponds to the results obtained using equations S22 and S23 (EISM). The first and second rows of Figure S7 display the projected thickness profiles for Inline XPCI and EISM, respectively, showing cases for W = 40 μm, and the three magnifications (M_{low}, M_{medium}, and M_{high}) across all voltages.

Contrast and CNR data for all cases are presented in Figure S8, while absorbed dose data are shown in Figure S9.

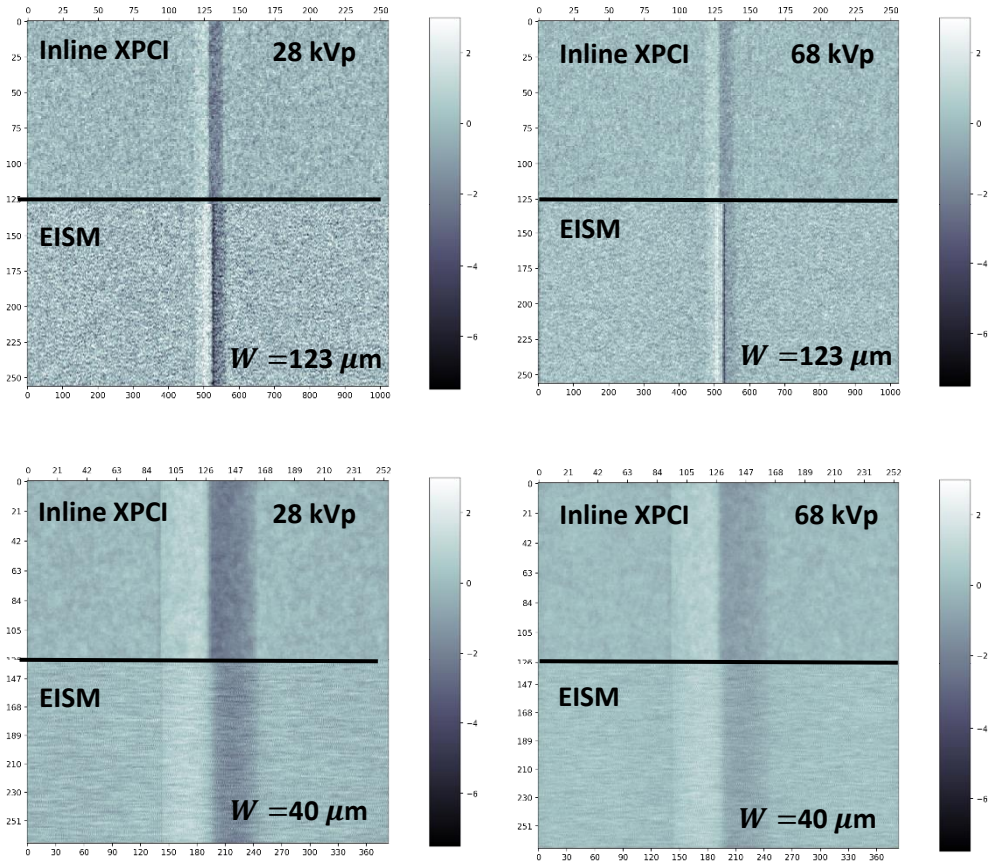

Figure S6. Projected thickness of the lumen at 28 kVp (first column) and 68 kVp (second column) for the focal spot of 30 μm and M_{high}. The top half shows retrieval for Inline XPCI, while the bottom half shows retrieval for EISM. The first and second rows correspond to W = 123 μm and W = 40 μm, respectively.

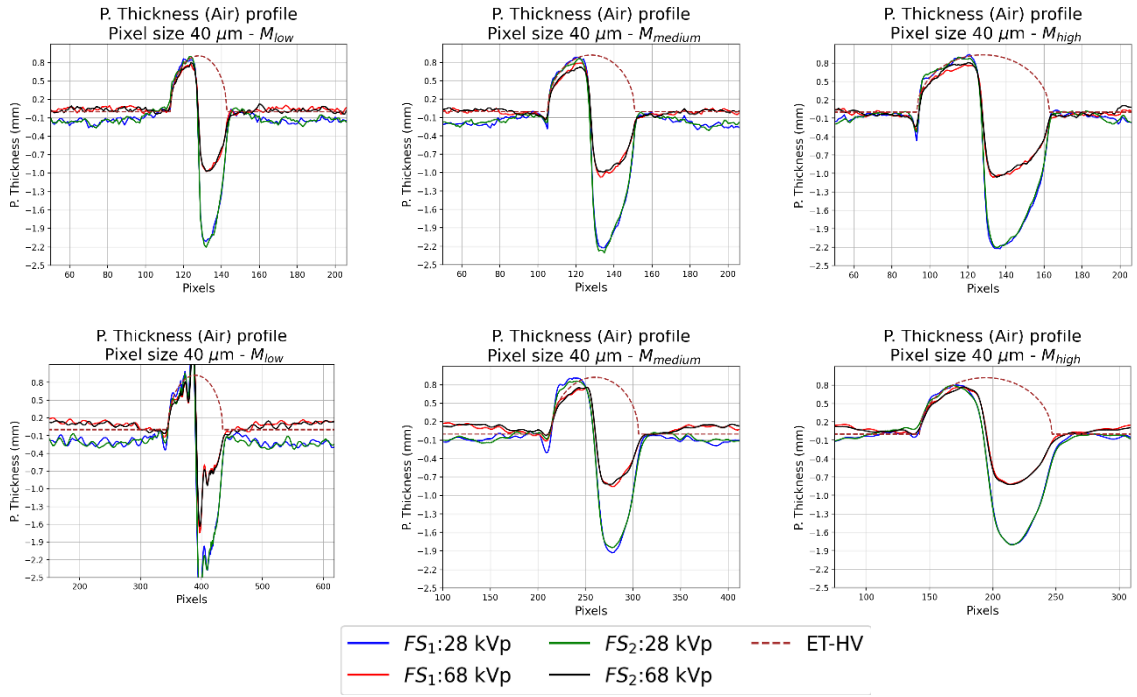

Figure S7. First (Second) row: Projected thickness profiles for Inline XPCI (EISM), showcasing results for $W = 40$ μm, and the three magnifications (M_{low}, M_{medium}, and M_{high}) across all voltages. The abbreviation FS_1 (FS_2) corresponds to the focal spot of 30 (50) μm.

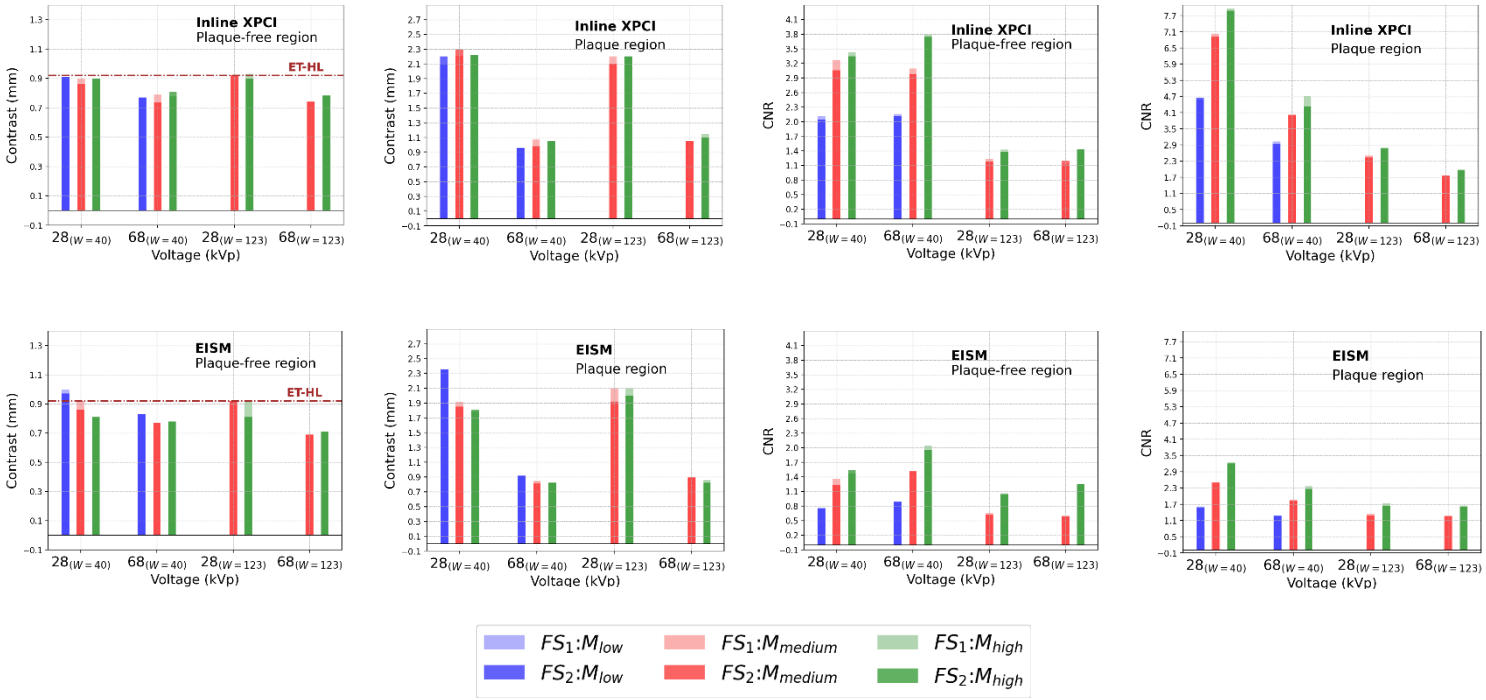

Figure S8. First (Second) row: Contrast and CNR variations using Inline XPCI (EISM) for the three magnifications across all voltages, pixel pitches and focal spots. The contrast and CNR values are evaluated in both the free-plaque region and the plaque region.

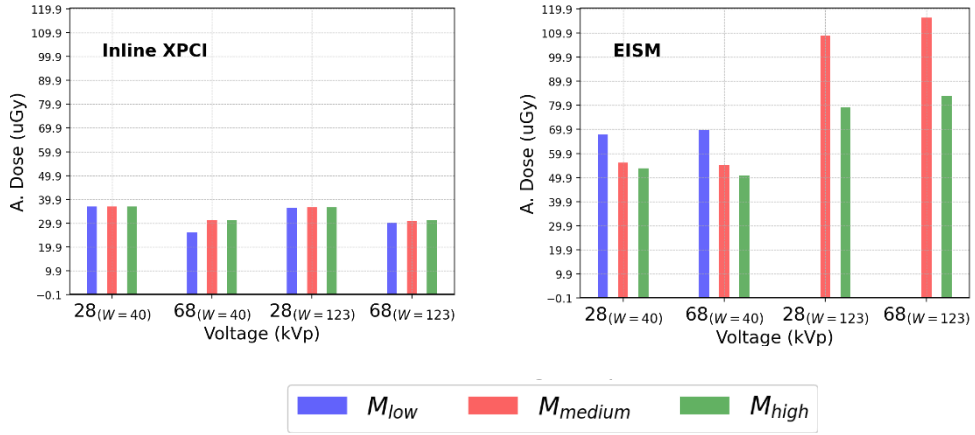

Figure S9. Absorbed dose across all magnifications, pixel pitches, and voltages are shown for Inline XPCI (left) and EISM (right).